Published in final edited form as:
ACS Chem Biol. 2012 June 15; 7(6): 1040–1048. doi:10.1021/cb300028a.

Selective Identification of Hedgehog Pathway Antagonists By Direct Analysis of Smoothened Ciliary Translocation

Yu Wang[1,2,4,6], **Anthony C. Arvanites**[1,3], **Lance Davidow**[1,3], **Joel Blanchard**[1,3,7], **Kelvin Lam**[1,3,8], **Jin Woo Yoo**[5], **Shannon Coy**[1,3,9], **Lee L. Rubin**[1,3,10], and **Andrew P. McMahon**[1,2,3,10]

[1]Department of Stem Cell and Regenerative Biology, Harvard University, Cambridge, MA 02138

[2]Department of Molecular and Cellular Biology, Harvard University, Cambridge, MA 02138

[3]Harvard Stem Cell Institute, Harvard University, Cambridge, MA 02138

[4]Department of Chemistry and Chemical Biology, Harvard University, Cambridge, MA 02138

[5]Harvard College, Harvard University, Cambridge, MA 02138

Abstract

Hedgehog (Hh) signaling promotes tumorigenesis. The accumulation of a membrane protein Smoothened (Smo) within the primary cilium (PC) is a key event in Hh signal transduction and many pharmacological inhibitors identified to date target Smo's actions. Smo ciliary translocation is inhibited by some pathway antagonists while others promote ciliary accumulation; an outcome that can lead to a hypersensitive state on renewal of Hh signaling. To identify novel inhibitory compounds acting on the critical mechanistic transition of Smo accumulation, we established a high content screen to directly analyze Smo ciliary translocation. Screening thousands of compounds from annotated libraries of approved drugs and other agents, we identified several new classes of compounds that block Sonic hedgehog-driven Smo localization within the PC. Selective analysis was conducted on two classes of Smo antagonists. One of these, DY131, appears to inhibit Smo signaling through a common binding site shared by previously reported Smo agonists and antagonists. Antagonism by this class of compound is competed by high doses of Smo-binding agonists such as SAG, and impaired by a mutation that generates a ligand independent, oncogenic form of Smo (SmoM2). In contrast, a second antagonist of Smo accumulation within the PC, SMANT, was less sensitive to SAG-mediated competition, and inhibited SmoM2 at similar concentrations to those that inhibit wild-type Smo. Our observations identify important differences among Hh antagonists and the potential for development of novel therapeutic approaches against mutant forms of Smo that are resistant to current therapeutic strategies.

Hedgehog (Hh) signaling plays an essential role in developmental processes and adult tissue homeostasis (1). An increasing body of evidence identifies the Hh pathway as a contributing factor in the growth of a variety of human cancers. The loss of normal regulatory control of the Hh pathway within a subset of Hh responsive cells leads directly to the initiation of

[10]Corresponding authors: Andrew McMahon, Tel: 617 496 3757, Fax: 617 496 3763, amcmahon@mcb.harvard.edu or Lee Rubin, Tel: 617 384 8105, Fax: 617 495 3961, lee_rubin@harvard.edu.
[6]Current address: The Morgridge Institute for Research, Madison, WI 53715;
[7]Current address: The Scripps Research Institute, Jupiter, Florida 33458;
[8]Current address: Blue Sky Biotech, Inc., Worcester, MA 01605;
[9]Current address: Dartmouth Medical School, Hanover, NH 03755; 10.

Author Contributions

Y. W, L.L.R and A.P.M conceived the project. Y. W. developed and validated the assay. All authors contributed in primary screens, secondary assays, and data analyses. Y.W., L.L.R., and A.P.M. wrote the paper.

particular solid tumors, notably basal cell carcinoma (BCC), the most prevalent cancer in the Caucasian population (2), and medulloblastoma (MB), the most common childhood brain cancer (3). In other cancers, Hh signals from tumor cells appear to condition the local environment to favor tumor growth. This category includes a broad spectrum of high incidence cancers, particularlythose in breast, lung, liver, stomach, pancreas, prostate, and gastro-intestinal tract (4–5). The potential of Hh targeted cancer therapy has stimulated an extensive search for Hh pathway antagonists. Typically, drug discovery screens have broadly sampled the Hh pathway looking for agents capable of silencing a Hh signal-dependent transcriptional response. Although small-molecule “hits” may occur at any point in the pathway that can ultimately translate into an altered transcriptional response, Smoothened (Smo), has emerged as the prevalent target. (6–7) Smo is essential for all pathway activity, and activating mutations in Smo have been observed in both human BCC and MB. Smo antagonists have entered clinical trials (8), andsuccessful repression of tumorigenesis in patients with invasive or metastatic forms of BCC has validated the concept of Hh targeted cancer therapy (9). The leading drug, GDC0449 (now marketed as Erivedge), was recently approved by the US Food and Drug Administration (FDA) for treatment of advanced BCC (10)(10)(10).

An obligatory step in the activation of Hh signaling is the accumulation of Smo in the primary cilium (PC), a tubulin-scaffolded membrane extension templated by the centriole (Supplementary Fig. 1). While all small molecule Smo agonists examined so far induce Smo accumulation in the PC, various Smo antagonists affect Smo localization in distinct ways (Supplementary Fig. 1) (11–13). SANT-1, SANT-2, and GDC0449 inhibit both Hh pathway activation and Sonic hedgehog (Shh) induced Smo accumulation within the PC (11–13). In contrast, Cyclopamine (cyc), a natural product from the plant *Veratrum californicum*, and its potent derivative KAAD-cyc, bind Smo and inhibit pathway activation, but behave as pseudo-agonists promoting Smo accumulation within the PC (11–14). Further, forskolin (FKL), a putative protein kinase A (PKA) activator, inhibits Hh pathway activity and indirectly promotes Smo ciliary accumulation through PKA stimulation (11). Thus, there are distinct actions and outcomes associated with different inhibitory factors grouped around Smo action (Supplementary Fig. 1). To explore regulatory activity at this critical level of pathway action, we performed a direct screen for inhibitors of Smo translocation to the PC and identified 20 classes of inhibitory compounds. We identified some novel compounds that may act on Smo in a similar manner to previously identified antagonists and agonists, underscoring the chemical diversity of compound interactions at what is possibly a common site. However, we also identified a new compound, SMANT, which inhibits an oncogenic form of Smo refractory to inhibition by currently available Smo antagonists.

Results

Screening for antagonists of Smo translocation to the primary cilium

In work to be published elsewhere, we have established a high content screen for modulators of Smo translocation focusing on small molecules stimulating Smo translocation to the PC (Wang Y. *et al.*, under revision). We then modified the system to identify inhibitors of Smo ciliary translocation. In brief, we developed a cell line producing human Smo::EGFP and Ivs::tagRFPT fusion proteins. Ivs::tagRFPT highlights the PC, and GFP enables the cellular trafficking of Smo to be visualized. Test compounds were added in low serum medium for 18–24 hours in the presence of Shh, cells were then fixed and stained with Hoechst (Supplementary Fig. 2). Quantitative multi-parametric image analyses were performed with custom algorithms (For details, please refer to Materials and Methods). The most critical parameters measured are indicated in Fig. 1a: Cell number was measured by counting Hoechst-labeled nuclei whereas the PC was precisely segmented as an Ivs::tagRFPT positive

structure; the specific PC localization of Smo::EGFP was discerned by applying a defined threshold for the length-width ratio of Ivs::tagRFPT positive structures (inset in Ivs::tagRFPT images) and then quantifying hSmo::EGFP intensity within the Ivs::tagRFPT positive PC. Key measurements from these analyses are shown for GDC0449 (Fig. 1b and c) and SANT-1 (Supplementary Fig. 3). As expected, each specifically inhibited Smo::EGFP accumulation in the PC without causing significant structural changes to the PC itself or measurable cytotoxicity (15–16).

We used this high content assay to screen a collection of approximately 5,600 small molecules for compounds that block Smo accumulation in the presence of Shh. The small molecule library includes FDA approved drugs, drug candidatesin preclinical or clinical development and a group of compounds with annotated biological activity. Representative examples of assay plates are shown (Supplementary Fig. 4). Z-prime scores (17) were consistently >0.6, confirming the robustnessof the screen.

We first eliminated small molecules with “off-target” effects, e.g. inhibitory effects on ciliary assembly/trafficking or general cytotoxicity. For example, HPI-4, a molecule that leads to truncation or loss of the PC (18), and vinblastine, a drug known to disrupt the assembly of microtubules (19), both appear as Hh pathway antagonists in a Gli-luciferase reporter assay (Fig. 2 a and c). However, the decrease in the Ivs::tagRFPT ciliary signal in the Smo high-content assay indicates a non-specific mechanism that alters PC structure (Fig. 2).

We identified 26 validated hits that could be divided into 20 classes. These hits include known Hh pathway inhibitors such as AntagVIII, a potent phenyl quinazolinone urea derivative (Supplementary Fig. 5)(20). Moreover, identification of AY9944, an inhibitor of cholesterol biosynthesis and esterification (21), adds additional support to the proposed intersection between cholesterol metabolism and the Hh pathway[26]. Hh ligands are covalently modified by cholesterol[27] and Hh trafficking has been linked to cholesterol transport processes (22–23),[29] but *in vitro* studies suggest the response of the target cell is actually suppressed when cholesterol biosynthesis is blocked (24). Our data suggest a potential link with Smo accumulation within the PC (Supplementary Fig. 6). Further, in line with a recent report (25), our screen identified itraconazole and ketoconazole, two anti-fungal drugs in current clinical use, as Smo inhibitors in the ciliary-based assay (Supplementary Fig. 7). In all cases examined, compounds that blocked Smo translocation to the PC inhibited Gli transcription activity (Supplementary Figs 5–7).

DY131 inhibits Smo signaling through a conventional mechanism

Of the novel compounds, we first selected DY131, a potent hit, for subsequent analysis. DY131, and its analog GSK4716, inhibited Shh induced accumulation of Smo::EGFP with IC50’s of 0.8 μM and 2μM respectively (Fig. 3a–c, Supplementary Fig. 8, Table 1). Both DY131 and GSK4716 inhibit Shh induced activation of a Glireporter with somewhat higher IC50’s (2μM and 10μM respectively) (Fig. 3d). The absence of an inhibitory activity in a Wnt pathway reporter assay argues for a specific action of DY131 in suppressing Shh action (Supplementary Fig. 9).

DY131 and GSK4716 were previously identified as agonists of the estrogen related receptors (ERR) (26–27). However, other ERR/ER ligands, including tamoxifen citrate, 4-hydroxytamoxifen (4-OHT), diethylstilbestrol, and hexestrol, did not alter the accumulation of Smo on the PC in either the presence or absence of Shh (Supplementary Fig. 10), arguing against an ERR-based mode of action for DY131 and GSK4716.

To investigate at what level DY131 functions in the Hh pathway, we compared the drug's dose-dependent performance in inhibiting the activities of wild-type Smo and SmoM2 (also named SMOA1), a constitutively active form of Smo with a tryptophan to leucine mutation in the 7th transmembrane domain (2). This mutation renders Smo markedly less sensitive (IC50's for SmoM2 are more than an order of magnitude higher than IC50's for wildtype Smo) to Cyc, SANT-1 and GDC0449-mediated inhibition (15–16, 28) (Supplementary Figs 11–12). When over-expressed, both wild-type Smo and SmoM2 constitutively localize to the primary cilium (6, 29). In contrast to its potent inhibition of the ciliary accumulation of wild-type Smo following exposure to Hh ligand (Fig. 3c), or over-expression of wild-type Smo (Fig. 3 e and f), DY131 failed to inhibit ciliary localization of SmoM2, or SmoM2 driven activation of transcriptional reporters of pathway activity, at doses up to 30μM (Fig. 3 e–g). However, DY131 suppressed SAG (100nM) induced accumulation of Smo::EGFP in the primary cilium and Gli transcription activity with an IC50 of approximately 2μM (Supplementary Fig. 13).

Interestingly, SANT-1 and GDC0449, at a dose high enough to block SmoM2 activity, did not alter SmoM2 ciliary accumulation, suggesting that, as with wild-type Smo, activity of this mutant can be abolished without blocking its localization to the PC (Supplementary Figs 11).

To determine if DY131 binds directly to Smo, we used a competition assay with bodipy-Cyc, a fluorescent analog of Cyc (30). Bodipy-Cyc specifically labels cells over-expressing Smo, co-expressing a red, nuclear fluorescent protein (Nuc-tagRFPT) marker, whereas SmoM2-expressing cells do not bind bodipy-Cyc, confirming the specificity of this assay (Fig. 3 h and i). DY131, like Cyc and SANT-1, acts as an effective competitor of bodipy-Cyc labeling of cells overexpressing Smo, consistent with either direct binding to Smo at the same site as bodipy-Cyc, or at another site on Smo resulting in allosteric modification and loss of bodipy-Cyc binding (Fig. 3 h and i).

SMANT inhibits Smo signaling with a novel mechanism

Our data suggest that DY131 and its analogs inhibit Hh signaling through a similar mechanism to inhibitors such as Cyc, SANT-1, and GDC0449. However, our focused effort in characterizing most potent hits from the screen also identified small molecules displaying novel behaviors. We named one compound, Smo Mutant ANTagonist (SMANT) as it exhibited an equivalent activity in inhibiting SmoM2 and wild-type Smo (Fig. 4a and h). SMANT and its analog SMANT-2 inhibited Shh induced ciliary accumulation of Smo::EGFP with IC50's of 1.1μM and 1.6μM, respectively (Fig. 4b and c; Table 1). Neither resulted in altered Ivs::tagRFPT localization at the PC or profound modulation of Wnt pathway activity consistent with a Hh pathway specific mode of action (Fig. 4b; Supplementary Fig. 14 and 15).

As with DY131, SANT-1, and GDC0449 (Fig. 3e and f, Supplementary Fig. 11), SMANT failed to block SmoM2::EGFP localization to the PC while potently inhibiting wild-type Smo accumulation (Fig. 4d and e). In contrast to some of the other Smo antagonists, SMANT failed to block Smo ciliary localization induced by SAG or Cyc (Fig. 4f and g; Supplementary Fig. 16; Supplementary Fig. 13a and b). However, in contrast to other pathway inhibitors, SMANT was similarly effective at inhibiting Smo and SmoM2 activity, and blocked the stimulatory action of SAG at different concentrations in the Gli-luciferase assay (Fig. 3d, 3g and 4h; Supplementary Fig. 12 and 13c). SMANT, like DY131 and GDC0449, and distinct from GANT61 (31), a known Gli inhibitor, does not alter Hh pathway activation induced by loss of suFU, a Gli regulatory factor (Fig. 4i), suggesting that SMANT functions at the Smo level. However, in contrast with strong competition between

DY131 and Cyc for binding Smo (Fig. 3h and i), SMANT was a poor competitor (Fig. 4j and k), consistent with a unique inhibitory action on Smo activity.

DY131 and SMANT effectively inhibit Hh signaling without the risk of rebound hyperactivity

To further explore the potential utility of compounds found in our assay for developing anti-cancer agents for Hh pathway targeted therapies, we tested DY131 and SMANT on cultured cerebellar granule neuron precursors (CGNPs) isolated from Ptch1+/− neonates. Constitutive activation of Hh signaling in these cells is associated with medulloblastoma (32). Consistent with their potency in inhibiting Hh activity in NIH/3T3 cells, DY131 and SMANT dramatically decreased phosphorylated histone H3 (pH3) marked proliferation of CGNPs induced by Shh (Fig. 5 a–b).

Finally, we primed cells with GDC0449, Cyc, FKL or SANT-1 at doses sufficient to decrease both Smo ciliary localization and Gli mediated transcription activity for 24 hours (Supplementary Fig. 1). Following the removal of drug containing medium, and extensive washing, cells were stimulated with either Hh ligand, or the direct-binding Smo agonist SAG (16, 33). As predicted, we observed an elevated signaling response specifically in Cyc and FKL treated cells (Supplementary Fig. 17a, Supplementary Fig. 18). The hypersensitivity to Hh pathway activation correlated with high levels of Smo that remained within the PC following removal of the antagonizing compound (Supplementary Fig. 17b–e). Next we tested the consequences of this effect for newly identified DY131 and SMANT using NIH3T3 cells (Fig. 5c) and CGNPs (Fig. 5 d–e). In contrast to Cyc, we observed no Shh driven hyperactivation of Hh pathway activity on removal of DY131 or SMANT in either the NIH3T3 Gliluciferase assay or the CGNP proliferation assay.

Discussion

Based on evidence presented here, compounds that inhibit both pathway activity and Smo accumulation in the primary cilium have characteristics that may make them reasonably preferred to antagonists that themselves promote ciliary accumulation of Smo. Therefore, the type of high content screen that we have established, which directly quantifies the Smo-PC interactions required for Hh pathway activity, is useful both for discovering new classes of antagonists, as well as for studying existing ones. The current screen, of over 5,000 compounds, selectively identified a substantial number of small molecules with efficacy in this assay, and more conventional Hh pathway assays. While careful analysis of DY131 suggests a direct interaction with Smo, SMANT shows a unique profile inhibiting an oncogenic form of Smo carrying the M2 mutation with similar efficacy to its wild-type counterpart. The differing properties of SMANT when compared with a variety of other Smo modulators (SAG, Cyc, GDC0449, and SANT-1) are consistent with a SMANT inhibitory action at a different site on Smo to that bound by these other compounds, or an indirect modulation of Smo activity. Smo can be inactivated in the PC by SMANT when harboring the M2 mutation, or after SAG driven translocation to the PC, suggesting that SMANT may inactivate both the oncogenic form and an SAG-bound form of Smo, and more importantly, the ciliary localization of Smo and its activation may be mechanistically divergent. It is possible that post-translational modifications, conformation changes, or interacting partners that regulate ciliary entry or accumulation of Smo differ from those governing activity in the primary cilium.(34–35) Frequently, compounds show a higher potency in the inhibition of Smo localization to the primary cilium than that in Gli-luciferase assays (Fig. 3c and d, Fig. 4 c and h, Supplementary Fig. 5–7). This could reflect pathway activity while Smo is out of the PC, or the different time frames involved in the two assay systems.

Our studies highlight new opportunities for therapeutic development that may potentiate existing approaches and over new strategies towards treatment of resistant forms of Smo emerging from somatic mutation. The screening platform provides a robust assay system. The Smo ciliary screen broadly interrogates a key aspect of HH pathway regulation and biology, and potentially identifies small molecule regulators that may not score in a conventional transcriptional end-point assay. These compounds may nevertheless provide a reasonable grounding for subsequent drug development. Further, the screen enables a stratification of small molecule function in the HH pathway and a platform that can be extended to potentially explore ciliopathies, an increasingly important area of medical significance (36).

Materials and Methods

Cell Culture

NIH/3T3 cells were maintained in DMEM containing 10%(v/v) calf serum, penicillin, streptomycin, and L-glutamine. HEK293, L, cos7, and suFU−/− mouse embryonic fibroblast cells were maintained in DMEM containing 10%(v/v) fetal bovine serum, penicillin, streptomycin, and L-glutamine. Smo::EGFP, SmoM2::GFP, and Ivs::tagRFPT were cloned into pBabe to generate retroviral particles for infection. Smo::EGFP/Ivs::tagRFPT and SmoM2::GFP/Ivs::tagRFPT stable cell lines were generated through viral infection of NIH/3T3 (13). A ShhLightII Gli reporter cell line was obtained from the American Type Culture Collection (ATCC) and used in luciferase reporter assays to measure Hh pathway activity. The cell line contains a stably integrated Gli-responsive Firefly luciferase reporter and a constitutive *Renilla* luciferase expression construct (28). Subclones expressing Smo or SmoM2 in ShhLightII cells were used for chemical epistasis analyses.

Shh conditioned medium, which is collected from cos7 cells transfected with an expression construct encoding the amino terminal 19kDa signaling peptide of Shh, was used at 13.7 (±3.0) nM. Wnt3a conditioned medium was collected from an L-cell line producingWnt3a ligand (37). Controls utilized supernatants from cells cos7 cells transfected with empty vector or a wild-type L-cell line.

Reagents

Cyclopamine and forskolin were purchased from Sigma. SAG, SANT-1, GDC0449, and BODIPY-cyclopamine were purchased from Axxora Platform, Tocris Biosciences, Selleck Chemicals, and Toronto Research Chemicals, respectively. All small molecule stock solutions were prepared by dissolving in DMSO at 10 mM and stored at −20°C. Mouse recombinant ShhN purified protein (IIShhN) was purchased from R&D Systems. Transfection was performed using Fugene 6 or Fugene HD from Roche.

Imaging Assays

Cells were cultured and treated in 384-well imaging plate precoated with poly-D-Lysine (Greiner Bio-one), fixed with 4%(w/v) paraformaldehyde (Electron Microscopy Sciences), and stained with Hoechst (Invitrogen). Images were collected using Opera High Content Screening System (Perkin Elmer). Activity Base (IDBS Inc,) and Pipeline Pilot (Accelrys, Inc.) were used for high content screening data management and analysis.

Image Analysis of Smo Ciliary Localization

Acapella 2.0 software (Evotec Technologies/PerkinElmer) was used to perform multi-parametric high content image quantification. Our image analysis script used Ivs::tagRFPT

to first determine the location of the PC and then Smo::EGFP to quantify the level of Smo present in the cilium.

First, we used the spot-finding algorithm in the RFP channel to find Ivs-rich spots. Each non-overlapping spot was based on a maximum 8 pixel-radius (when using a 40x objective) around a central intensity peak of 5 pixels. A distance of at least 10 pixels was required between adjacent spot centers. Spot peaks had to exceed thresholds of relative intensity compared to the remaining body of the spot as well as to the entire image. The average, maximum and total RFP intensity of each spot were measured. The spots with sufficiently high absolute maxima to pass the selected threshold were classified as positive spots. To form candidate cilia, we selected the brightest 15% of the pixels in each positive spot and merged those pixels into objects so that the brightest parts of adjacent spots could form single, larger cilia-shaped objects. To qualify the candidate cilia as true Ivs-positive cilia, the width of the objects created from merging the brightest pixels in each spot had to be at least 2 pixels and the length to half-width ratio had to exceed 3. (i.e. a 3-pixel long by 2-pixel wide cilium was the minimum accepted cilium size and the length had to be at least 1.5 fold of the width). The mean GFP intensity within these Ivs-positive cilia was used to estimate the ciliary level of Smo protein. We found it necessary to subtract the background of the mean GFP intensity in the 3-pixel wide area around each candidate cilium to avoid some false positives. Those Ivs-positive cilia that exceed the final mean GFP intensity threshold set for each experiment were deemed Smo-positive cilia.

Hoechst staining was used to determine the total number of nuclei per well. The final output measurements of the number of Ivs-positive cilia in the well, the number of Smo-positive cilia in the well and the mean GFP intensity of the accepted cilia within the well were used to calculate if a compound qualified as an inhibitor and to estimate the quality of inhibition. Inhibitors of smoothened accumulation into the cilia were initially chosen as compounds that had numbers of Ivs-positive cilia per nucleus (or per field of view) similar to the DMSO controls, but fewer Smo-positive cilia compared to the DMSO controls. Compounds that generated many fewer Ivs-positive cilia were judged as either defective in cilium assembly/trafficking or generally toxic depending on the morphology of the cells. Measurements of the geometry of the cilia as well as the total fluorescent intensities of each cilium in the Smo- and Ivs- channels were used to determine if any of the compounds were having unusual effects on cilia size, intensity or frequency of observation or combinations of all three characteristics.

The thresholds and parameters used in selecting, classifying, and quantitating spots, candidate cilia and nuclei, were applied uniformly for every well in each set of plates prepared as a single batch with the same set of cells and reagents. We used diagnostic images during threshold selection to outline which objects (spots, candidate cilia, candidate nuclei etc) passed or failed each selection. At least 2 fields of positive controls (Shh +SANT-1) and negative controls (Shh+DMSO) were examined for threshold setting. Visual observation and Z-prime calculations measuring the ability of the assay to distinguish positive from negative controls were used for quality control on each batch of plates and set of thresholds. All the images for comparison were scanned with identical microscopic settings and analyzed with the same input parameters.

Hh and Wnt activity assays

Hh activity assays were performed using ShhLightII cells, Smo/LightII cells, SmoM2/LightII cells, and suFU−/− mouse embryonic fibroblasts. In the suFU−/− cells, Hh activity was measured after co-transfection with Gli driven firefly luciferase and TK-renilla luciferase reporters (38). Wnt activity was measured in 293 cells co-transfected with Top-flash and TK-renilla luciferase reporters (39). Cells were cultured and treated in 96 well

assay plates (Corning) and incubated with Duo-Glo luciferase substrates (Promega) to measure firefly and renilla luciferase activity sequentially using a TopCount NX Microplate Scintillation and Luminescence Counter (Perkin Elmer). The renilla luciferase signal was used to normalize the firefly reporter activity.

Bodipy-Cyclopamine Competition Assays

Cos7 cells were transfected with a plasmid co-expressing *Smo* and a nuclear localized form of tagRFPT (pCIT-Smo). An empty parental construct (pCIT), and a construct that co-expresses *SmoM2*, were used as controls to assess specificity and background noise. Three days after transfection, cells were incubated with 5 nM Bodipy-cyclopamine, with or without other compounds for 1 hour at 37°C. Cells were washed, fixed and stained with Hoechst. Images were collected by an Opera High Content Screen System. Bodipy fluorescence was quantified specifically for transfected cells (determined by red tagRFPT+ nucleus) using a program developed by the authors with Acapella 2.0 software. All of the images were scanned with identical microscopic settings and analyzed with the same input parameters.

CGNP proliferation Assays

CGNP primary cells were isolated from P7 *Ptch1*+/− mice as previously reported (40) and immediately seeded in poly-D-lysine coated imaging plates (Greiner Bio-one). Compounds were applied 2 hours post seeding, for either 36 (Fig. 5a–b) or 72 hours (Fig. 5d–e). After completion of each experimental regimen, cells were fixed with 4% paraformaldehyde (Electron Microscopy Sciences), and stained with anti-pH3 antibody (Upstate; 1:100) followed by a secondary antibody (Invitrogen) and Hoechst (Invitrogen). Images were then collected using a confocal microscope. Cell proliferation, as marked by a pH3 signal, was quantified with an in-house program developed by the authors using Acapella 2.0 software. Identical microscopic settings were used in each analysis and identical input parameters were implemented for each experiment.

Supplementary Material

Refer to Web version on PubMed Central for supplementary material.

Acknowledgments

We are very grateful to C. T. Walsh, S.L. Schreiber, A. Saghatelian, and T. Curran for critical review of our results and helpful discussions. We thank J.W. Lichtman, R.Y. Tsien, M.P. Scott, and P.T. Chuang for sharing reagents. We thank R. A. Segal and X. Zhao for technical assistance on CNGP cell culture and our colleagues in the McMahon and Rubin laboratories for support on our research. We are also grateful to R. Hellmiss at Harvard Center of Biological Imaging for help on artwork. This work was supported by a grant from Harvard Stem Cell Institute (DP-0033-08-02 to A.P.M and L.L.R) and a grant from National Institutes of Health (R37 NS033642 to A.P.M). Y.W, L.L.R and A.P.M hold patent positions around Hedgehog signaling and drug discovery platforms.

References

1. McMahon AP, Ingham PW, Tabin CJ. Developmental roles and clinical significance of hedgehog signaling. Curr Top Dev Biol. 2003; 53:1–114. [PubMed: 12509125]
2. Xie J, Murone M, Luoh SM, Ryan A, Gu Q, Zhang C, Bonifas JM, Lam CW, Hynes M, Goddard A, Rosenthal A, Epstein EH Jr, de Sauvage FJ. Activating Smoothened mutations in sporadic basal-cell carcinoma. Nature. 1998; 391:90–92. [PubMed: 9422511]
3. Romer JT, Kimura H, Magdaleno S, Sasai K, Fuller C, Baines H, Connelly M, Stewart CF, Gould S, Rubin LL, Curran T. Suppression of the Shh pathway using a small molecule inhibitor eliminates medulloblastoma in Ptc1 (+/−) p53 (−/−) mice. Cancer Cell. 2004; 6:229–240. [PubMed: 15380514]

4. Yauch RL, Gould SE, Scales SJ, Tang T, Tian H, Ahn CP, Marshall D, Fu L, Januario T, Kallop D, Nannini-Pepe M, Kotkow K, Marsters JC, Rubin LL, de Sauvage FJ. A paracrine requirement for hedgehog signalling in cancer. Nature. 2008; 455:406–410. [PubMed: 18754008]
5. Rubin LL, de Sauvage FJ. Targeting the Hedgehog pathway in cancer. Nature Reviews Drug Discovery. 2006; 5:1026–1033.
6. Corbit KC, Aanstad P, Singla V, Norman AR, Stainier DYR, Reiter JF. Vertebrate Smoothened functions at the primary cilium. Nature. 2005; 437:1018–1021. [PubMed: 16136078]
7. Rohatgi R, Milenkovic L, Scott MP. Patched1 regulates hedgehog signaling at the primary cilium. Science. 2007; 317:372–376. [PubMed: 17641202]
8. Scales S, de Sauvage F. Mechanisms of Hedgehog pathway activation in cancer and implications for therapy. Trends Pharmacol Sci. 2009; 6:303–312. [PubMed: 19443052]
9. Von Hoff D, Lorusso P, Rudin C, Reddy J, Yauch R, Tibes R, Weiss G, Borad M, Hann C, Brahmer J, Mackey H, Lum B, Darbonne W, Marsters J, de Sauvage F, Low J. Inhibition of the Hedgehog Pathway in Advanced Basal-Cell Carcinoma. N Engl J Med. 2009; 361:1164–1172. [PubMed: 19726763]
10. Allison M. Hedgehog hopes lifted by approval..and stung by failure. Nat Biotechnol. 2012; 30:203. [PubMed: 22398601]
11. Wilson CW, Chen M-H, Chuang P-T. Smoothened adopts multiple active and inactive conformations capable of trafficking to the primary cilium. PLoS ONE. 2009; 4:e5182. [PubMed: 19365551]
12. Rohatgi R, Milenkovic L, Corcoran R, Scott M. Hedgehog signal transduction by Smoothened: Pharmacologic evidence for a 2-step activation process. Proc Natl Acad Sci USA. 2009; 106:3196–3201. [PubMed: 19218434]
13. Wang Y, Zhou Z, Walsh C, McMahon A. Selective translocation of intracellular Smoothened to the primary cilium in response to Hedgehog pathway modulation. Proc Natl Acad Sci USA. 2009; 106:2623–2628. [PubMed: 19196978]
14. Dijkgraaf GJ, Alicke B, Weinmann L, Januario T, West K, Modrusan Z, Burdick D, Goldsmith R, Robarge K, Sutherlin D, Scales SJ, Gould SE, Yauch RL, de Sauvage FJ. Small molecule inhibition of GDC-0449 refractory smoothened mutants and downstream mechanisms of drug resistance. Cancer Res. 2011; 71:435–444. [PubMed: 21123452]
15. Yauch R, Dijkgraaf G, Alicke B, Januario T, Ahn C, Holcomb T, Pujara K, Stinson J, Callahan C, Tang T, Bazan J, Kan Z, Seshagiri S, Hann C, Gould S, Low J, Rudin C, de Sauvage F. Smoothened Mutation Confers Resistance to a Hedgehog Pathway Inhibitor in Medulloblastoma. Science. 2009; 326:572–574. [PubMed: 19726788]
16. Chen JK, Taipale J, Young KE, Maiti T, Beachy PA. Small molecule modulation of Smoothened activity. Proc Natl Acad Sci USA. 2002; 99:14071–14076. [PubMed: 12391318]
17. Zhang JH, Chung TDY, Oldenburg KR. A simple statistical parameter for use in evaluation and validation of high throughput screening assays. Journal of Biomolecular Screening. 1999; 4:67–73. [PubMed: 10838414]
18. Hyman J, Firestone A, Heine V, Zhao Y, Ocasio C, Han K, Sun M, Rack P, Sinha S, Wu J, Solow-Cordero D, Jiang J, Rowitch D, Chen J. Small-molecule inhibitors reveal multiple strategies for Hedgehog pathway blockade. Proc Natl Acad Sci USA. 2009; 106:14132–14137. [PubMed: 19666565]
19. Jordan MA, Wilson L. Microtubules as a target for anticancer drugs. Nature Reviews Cancer. 2004; 4:253–265.
20. Brunton SA, Stibbard JHA, Rubin LL, Kruse LI, Guicherit OM, Boyd EA, Price S. Potent inhibitors of the hedgehog signaling pathway. Journal of Medicinal Chemistry. 2008; 51:1108–1110. [PubMed: 18275133]
21. Incardona JP, Eaton S. Cholesterol in signal transduction. Current Opinion in Cell Biology. 2000; 12:193–203. [PubMed: 10712926]
22. Lewis PM, Dunn MP, McMahon JA, Logan M, Martin JF, St-Jacques B, McMahon AP. Cholesterol modification of sonic hedgehog is required for long-range signaling activity and effective modulation of signaling by Ptc1. Cell. 2001; 105:599–612. [PubMed: 11389830]

23. Li YN, Zhang HM, Litingtung Y, Chiang C. Cholesterol modification restricts the spread of Shh gradient in the limb bud. P Natl Acad Sci USA. 2006; 103:6548–6553.
24. Cooper MK, Wassif CA, Krakowiak PA, Taipale J, Gong R, Kelley RI, Porter FD, Beachy PA. A defective response to Hedgehog signaling in disorders of cholesterol biosynthesis (vol 33, pg 508, 2003). Nature Genetics. 2003; 34:113–113.
25. Kim J, Tang JY, Gong R, Lee JJ, Clemons KV, Chong CR, Chang KS, Fereshteh M, Gardner D, Reya T, Liu JO, Epstein EH, Stevens DA, Beachy PA. Itraconazole, a commonly used antifungal that inhibits Hedgehog pathway activity and cancer growth. Cancer Cell. 2010; 17:388–399. [PubMed: 20385363]
26. Yu DD, Forman BM. Identification of an agonist ligand for estrogen-related receptors ERRbeta/gamma. Bioorg Med Chem Lett. 2005; 15:1311–1313. [PubMed: 15713377]
27. Zuercher WJ, Gaillard S, Orband-Miller LA, Chao EY, Shearer BG, Jones DG, Miller AB, Collins JL, McDonnell DP, Willson TM. Identification and structure-activity relationship of phenolic acyl hydrazones as selective agonists for the estrogen-related orphan nuclear receptors ERRbeta and ERRgamma. J Med Chem. 2005; 48:3107–3109. [PubMed: 15857113]
28. Taipale J, Chen JK, Cooper MK, Wang B, Mann RK, Milenkovic L, Scott MP, Beachy PA. Effects of oncogenic mutations in Smoothened and Patched can be reversed by cyclopamine. Nature. 2000; 406:1005–1009. [PubMed: 10984056]
29. Han Y-G, Spassky N, Romaguera-Ros M, Garcia-Verdugo J-M, Aguilar A, Schneider-Maunoury S, Alvarez-Buylla A. Hedgehog signaling and primary cilia are required for the formation of adult neural stem cells. Nat Neurosci. 2008; 11:277–284. [PubMed: 18297065]
30. Chen JK, Taipale J, Cooper MK, Beachy PA. Inhibition of Hedgehog signaling by direct binding of cyclopamine to Smoothened. Genes Dev. 2002; 16:2743–2748. [PubMed: 12414725]
31. Lauth M, Bergström A, Shimokawa T, Toftgård R. Inhibition of GLI-mediated transcription and tumor cell growth by small-molecule antagonists. Proc Natl Acad Sci USA. 2007; 104:8455–8460. [PubMed: 17494766]
32. Schuller U, Heine VM, Mao J, Kho AT, Dillon AK, Han YG, Huillard E, Sun T, Ligon AH, Qian Y, Ma Q, Alvarez-Buylla A, McMahon AP, Rowitch DH, Ligon KL. Acquisition of granule neuron precursor identity is a critical determinant of progenitor cell competence to form Shh-induced medulloblastoma. Cancer Cell. 2008; 14:123–134. [PubMed: 18691547]
33. Frank-Kamenetsky M, Zhang XM, Bottega S, Guicherit O, Wichterle H, Dudek H, Bumcrot D, Wang FY, Jones S, Shulok J, Rubin LL, Porter JA. Small-molecule modulators of Hedgehog signaling: identification and characterization of Smoothened agonists and antagonists. J Biol. 2002; 1:10. [PubMed: 12437772]
34. Chen Y, Sasai N, Ma G, Yue T, Jia J, Briscoe J, Jiang J. Sonic Hedgehog dependent phosphorylation by CK1alpha and GRK2 is required for ciliary accumulation and activation of smoothened. PLoS Biol. 2011; 9:e1001083. [PubMed: 21695114]
35. Su Y, Ospina JK, Zhang J, Michelson AP, Schoen AM, Zhu AJ. Sequential phosphorylation of smoothened transduces graded hedgehog signaling. Sci Signal. 2011; 4:ra43. [PubMed: 21730325]
36. Nigg EA, Raff JW. Centrioles, centrosomes, and cilia in health and disease. Cell. 2009; 139:663–678. [PubMed: 19914163]
37. Willert K, Brown JD, Danenberg E, Duncan AW, Weissman IL, Reya T, Yates JR 3rd, Nusse R. Wnt proteins are lipid-modified and can act as stem cell growth factors. Nature. 2003; 423:448–452. [PubMed: 12717451]
38. Nybakken K, Vokes SA, Lin TY, McMahon AP, Perrimon N. A genome-wide RNA interference screen in Drosophila melanogaster cells for new components of the Hh signaling pathway. Nature Genetics. 2005; 37:1323–1332. [PubMed: 16311596]
39. Corbit KC, Shyer AE, Dowdle WE, Gaulden J, Singla V, Reiter JF. Kif3a constrains beta-catenin-dependent Wnt signalling through dual ciliary and non-ciliary mechanisms. Nat Cell Biol. 2008; 10:70–76. [PubMed: 18084282]
40. Chan JA, Balasubramanian S, Witt RM, Nazemi KJ, Choi Y, Pazyra-Murphy MF, Walsh CO, Thompson M, Segal RA. Proteoglycan interactions with Sonic Hedgehog specify mitogenic responses. Nature Neuroscience. 2009; 12:409–417.

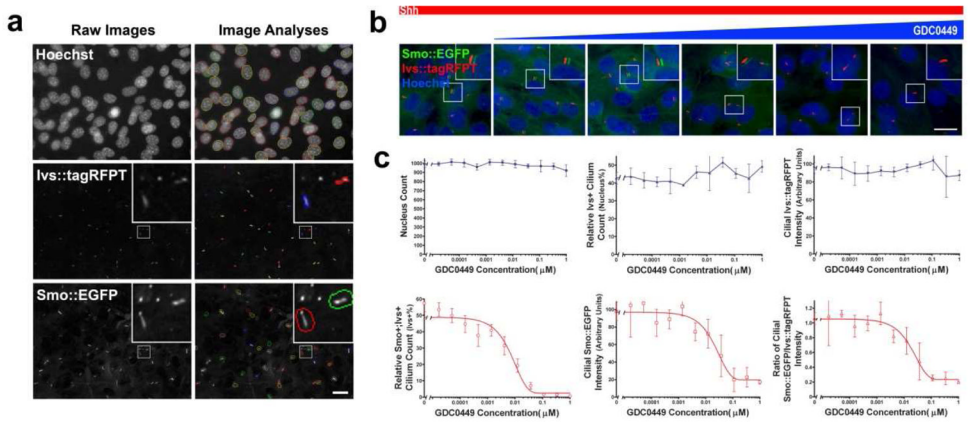

Fig. 1.

A high content Smo antagonist screen - image analysis and assay validation.**(a)** A field of cells in a typical well. The cell number was calculated by counting Hoechst stained nuclei. The PC were precisely segmented as Ivs::tagRFPT positive structures and hSmo::EGFP intensity was quantified in the PC. **(b)** Representative images of the dose-dependent inhibition of Smo::EGFP ciliary accumulation by GDC0449. The concentrations of GDC0449 used to obtain these images were 0, 0.15nM, 1.3nM, 12nM, 111nM, 1μM from left to right. Scale bar: 10μm. **(c)** Key measurements from high content image analyses. The cell number was determined by counting Hoechst stained nuclei. Ivs::tagRFPT positive structures were precisely segmented as the PC and Smo::EGFP intensity within the PC was quantified. The Ivs+ cilium count and Smo+ cilium count were determined based on arbitrary thresholds; the mean (±S.D) shown is based on four replicates.

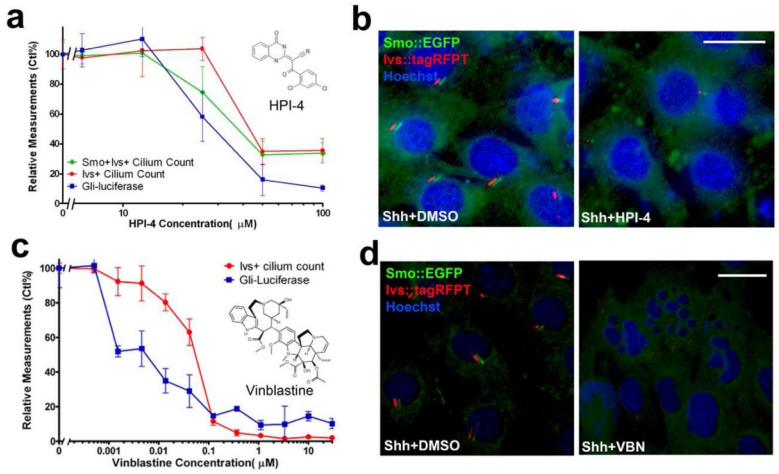

Fig. 2.

Identification of compounds disrupting the PC. **(a–b)** HPI-4, an inhibitor of ciliogenesis, was identified in the assay. Please note that, throughout this paper, Ctrl% is an additional normalization over the mean of DMSO (with or without Shh) treatment as 100%, unless stated otherwise, such as "Ctl=1".**(c–d)** Vinblastine (VBN), which disrupts microtubules, and leads to disruption of the PC, was also identified through general effects on Ivs::tagRFPt; the mean (±S.D) for the Smo localization assay and Gli-luciferase transcriptional reporter assays was calculated from four replicates (a and c). HPI-4 and VBN were used at 50μM and 370nM, respectively, to generate the representative images in (b) and (d). Scale bar: 10μm.

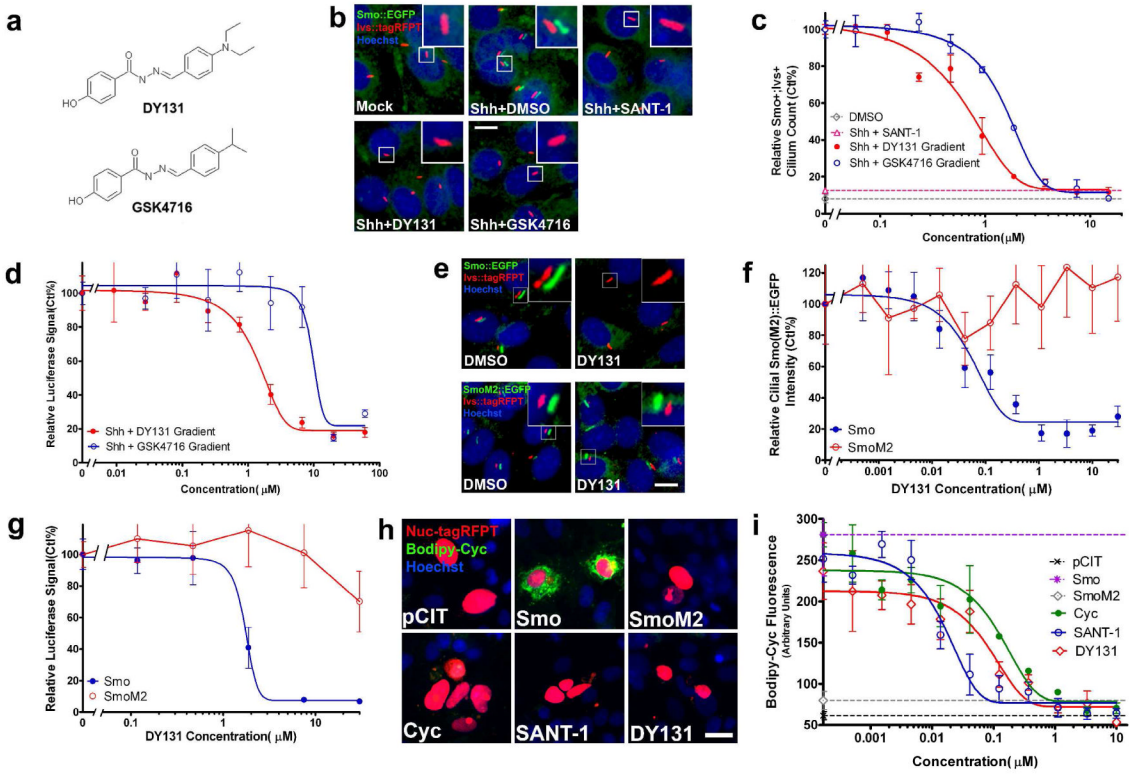

Fig. 3.

DY131 displays a conserved mechanism for Smo inhibition similar with previously identified antagonists. **(a)** Structure of DY131 and GSK4716. **(b–c)** Representative images (b) and quantification (c) of DY131 and GSK4716 inhibition of Hh induced Smo accumulation at the primary cilium. 500nM SANT-1 was used as a positive controlfor pronounced inhibition. DY131 and GSK4716 were used at 3.75μM and 7.5μM, respectively, for data in (b). Scale bar: 5μm. **(d)** Gli-luciferase measurements indicate dose-dependent inhibition of Hh pathway activity by both DY131 and GSK4716. Data show the means (±S.D.) from quadruplicate samples. Image analysis was based on over 300 cells per sample. **(e)** Representative images showing Smo::EGFP and SmoM2::EGFP overexpressing cells treated with vehicle or 1.1μM DY131. Scale bar: 5μm. **(f)** Image analysis of quadruplicate samples, plotting mean (±S.D.) of over 300 cells analyzed in each sample. **(g)** Dose-response curves displaying DY131 inhibition of wild-type Smo, and SmoM2 activity. Data show mean (±S.D.) in quadruplicate samples. Representative images **(h)** and quantification **(i)** of Bodipy-Cyc competition experiments. Cyc, SANT-1, and DY131 were each used at 1.1 μM in (h). Scale bar: 10μm. Data show the mean (±S.D.) in quadruplicate samples (i), analyzing 50–100 transfected cells in each sample.

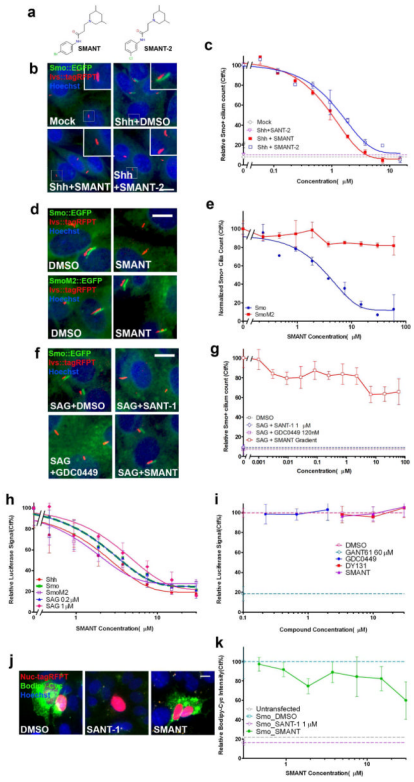

Fig. 4.

SMANT displays an unprecedented mechanism for Smo inhibition. **(a)** Structure of SMANT and SMANT-2. **(b–c)** Representative images (b) and quantification (c) of SMANT and SMANT-2 inhibition of Hh induced Smo accumulation at the primary cilium. 1μM SANT-2 was used as a positive control. SMANT and SMANT-2 were used at 7.5μM for data in (b). Scale bar: 5μm. **(d)** Representative images showing Smo::EGFP and SmoM2::EGFP overexpressing cells treated with vehicle or SMANT. SMANT was applied to wild-type Smo and SmoM2 expressing cells at 7.5μM and 30μM respectively. Scale bar: 5μm. **(e)** Image analysis of quadruplicate samples shown in (d), plotting mean (±S.D.) of over 300 cells analyzed in each sample. **(f–g)** Representative images (f) and quantifications of Smociliary localization (g) showing Smo::EGFP/Ivs::tagRFPT cells treated with 100nM SAG combined with vehicle, SANT-1, GDC0449, or SMANT. SANT-1, GDC0449 and SMANT were used at 1μM, 120nM, and 60μM. **(h)** Gli-luciferase measurement of dose-dependent inhibition of Hh pathway activity by SMANT upon Shh stimulation, overexpression of Smo and SmoM2 respectively, or treatment with 0.2 μM or 1μM of SAG. Data show the means (±S.D.) from triplicate samples. **(i)** Gli-luciferase measurements in suFU−/− mouse embryonic fibroblasts treated with DY131 and SMANT respectively. GDC0449 and GANT61 were used as negative and positive controls respectively. **(j–k)** Representative images (j) and quantification (k) of Bodipy-Cyc competition experiments for SMANT. SANT-1 served as a control for competition activity. SMANT was used at 30 μM in (h). Scale bar: 5μm. Data show the mean (±S.D.) from quadruplicate samples (i), analyzing 100–200 transfected cells in each sample.

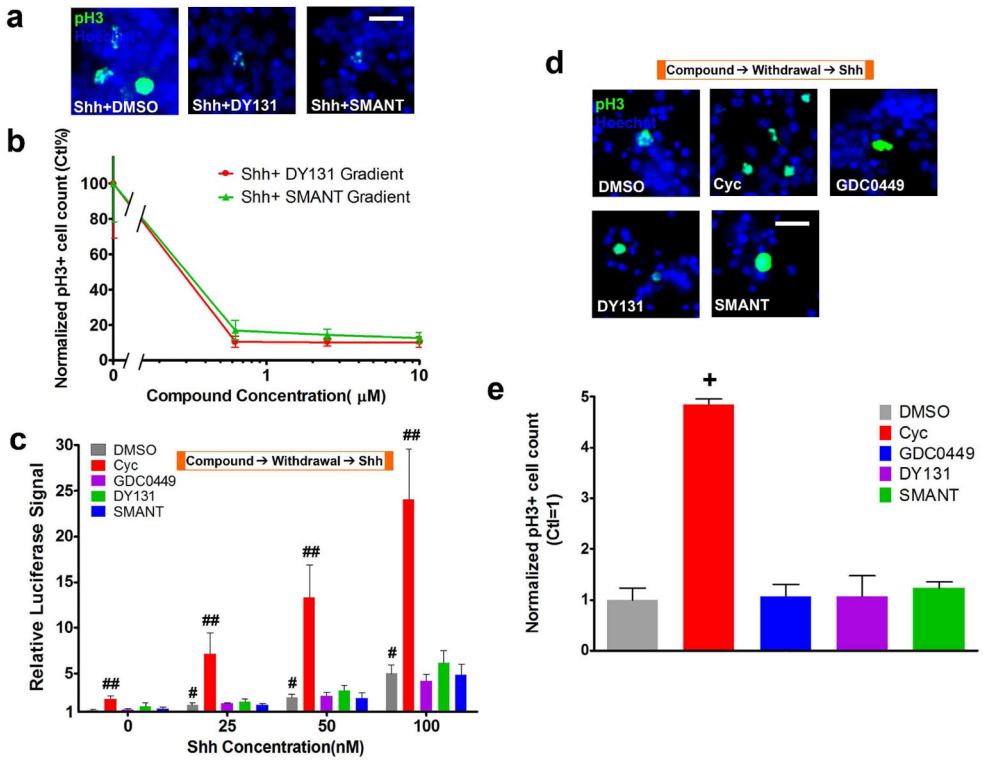

Fig. 5.

DY131 and SMANT inhibit proliferation of cerebellar granule-cell neural progenitors (CGNP) without conferring hypersensitivity to Shh stimulation. **(a–b)** representative images (a) and quantification of phospho-histone H3 (pH3) positive cells (b) upon co-treatment with 0.625μM DY131 or SMANT with Shh ligand. (b) P<=0.001 in t-test for all samples treated with DY131 or SMANT at 0.625μM and above compared with DMSO treated controls. **(c–e)** In contrast to Cyc, GDC0449, DY131, and SMANT do not confer prolonged hypersensitivity to Shh stimulation in either Gli responsive reporter (c) or CGNP proliferation assays (d–e). Hh signaling activity and CGNP proliferation were measured after treatment with vehicle, Cyc (5μM), GDC0449 (500nM), DY131 (10μM), or SMANT (10μM) separately. Samples were analyzed in quadruplicate; data show the mean (±S.D.). For the Gli-luciferase reporter assay (c), cells stimulated by Shh for a relatively short time period (12 hours) displayed a modest but significant inductive response (#p<0.003 in a t test comparing to a DMSO primed 0 nM Shh treatment). The response was enhanced by pre-treating cells with Cyc (##P<0.003 in t test comparing to DMSO priming and stimulation with the same concentration of Shh) whereas pretreatment with GDC0449, DY131, or SMANT showed no enhancing activity (P>0.05 in t test comparing samples primed with DMSO and stimulated with the same concentration of Shh). For the CGNP assay (d–e), cells were treated for 3 days. +p<0.0001 in a t test comparing the effects of DMSO (control) or any of the antagonists of Smo ciliary accumulation.

Table 1

IC50's of newly identified Smo antagonists in various cell based assays. Please note that IC50's in this paper were obtained through non-linear regression based on the following equation: $Y=\mathrm{Bottom}+(\mathrm{Top}-\mathrm{Bottom})/(1+10^{\wedge}((\mathrm{X}-\mathrm{LogIC50})))$, where the top and bottom are the Y values of plateaus of no inhibition and saturated inhibition separately.

Cell Line	Stimulus	Measurement	DY131	SMANT
3T3/Smo::GFP/Ivs::tagRFPT	Shh	Inhibition of Shh-induced Smo::GFP ciliary accumulation	0.8	1.1
3T3/Shh-LightII	Shh	Inhibition of Shh-induced expression of Gli-luciferase reporter	2	2
3T3/Smo::GFP/Ivs::tagRFPT	SAG	Inhibition of SAG-induced Smo::GFP ciliary accumulation	2 (100nM SAG)	>60 (100 nM SAG)
3T3/Shh-LightII	SAG	Inhibition of SAG-induced expression of Gli-luciferase reporter	2 (100nM SAG)	3 (200n M SAG); 4 (1 μM SAG)
3T3/Smo::GFP Overexpression/Ivs::tagRFPT	None	Inhibition of ciliary accumulation of Smo::GFP upon overexpression	0.08	3
3T3/Smo::GFP Overexpression/Shh-LightII	None	Inhibition of expression of Gli-luciferase reporter induced by Smo::GFP overexpression	>30	3
3T3/SmoM2::GFP Overexpression/Ivs::tagRFPT	None	Inhibition of ciliary localization of SmoM2::GFP	>30	>60
3T3/ SmoM2::GFP Overexpression/Shh-LightII	None	Inhibition of expression of Gli-luciferase reporter induced by SmoM2::GFP overexpression	>30	1.2
Cos7/Smo expression	None	Competition of BODIPY-cyclopamine-Smo binding	0.1	>30
Ptch1+/− CGNP	Shh	Shh induced cell proliferation marked by pH3	<0.625	<0.625